RSC Advances

PAPER

View Article Online
View Journal | View Issue

Open Access Article. Published on 23 January 2019. Downloaded on 1/13/2026 11:41:34 AM.
This article is licensed under a Creative Commons Attribution-NonCommercial 3.0 Unported Licence.

Check for updates

Cite this: *RSC Adv.*, 2019, **9**, 2967

Comparison of hypoglycemic effects of ripened pu-erh tea and raw pu-erh tea in streptozotocin-induced diabetic rats†

Qianzhi Ding,[a] Wei Zheng,[a] Bowei Zhang,[b] Xiaojuan Chen,[a] Jie Zhang,[a] Xu Pang,[a] Yong Zhang,[c] Dexian Jia,[c] Surui Pei,[d] Yuesheng Dong[b] and Baiping Ma *[a]

Received 9th November 2018
Accepted 14th January 2019

DOI: 10.1039/c8ra09259a

rsc.li/rsc-advances

Pu-erh tea is produced from the leaves of large-leaf tea species (*Camellia sinensis* var. assamica) in the Yunnan province of China and divided into ripened pu-erh tea (RIPT, with pile-fermentation) and raw pu-erh tea (RAPT) according to processing methods. RIPT extract showed more potent anti-diabetic effects on two-hour postprandial blood glucose (2h-PBG) and fasting blood glucose (FBG) than RAPT extract. UHPLC-Q-TOF/MS and UHPLC-PDA analyses found that 17 newly formed components and the increased components after fermentation, such as quinic acid, gallic acid, caffeine, puerin I and so on, might be the main contributors to the enhanced activities of RIPT. In addition, the probiotic role of RIPT to some beneficial gut bacteria, such as *lactobacillus*, *Prevotellaceae NK3B31 group*, *Alloprevotella* and *Prevotella*, was observed in our study. These results might provide a clue to anti-diabetic mechanism and active components of pu-erh tea, and use as a functional beverage worth to be further studied.

1 Introduction

Diabetes mellitus is a complex metabolic disorder, which has become a growing global health problem and caused increasing premature mortality and healthcare costs.[1] According to the International Diabetes Federation, there are an estimated 451 million individuals (age from 18 to 99) suffering from diabetes, and the number is predicted to be 693 million by 2045. The estimated healthcare expenditure relating to diabetes reached 850 billion USD for adults in 2017.[2] Therefore, looking for anti-diabetic functional foods, which might have low side-effects and low cost, has a significance to global health.

Tea is one of the most popular world-wide beverages and has various biological activities.[3,4] In recent years, pu-erh tea becomes more and more popular in Southeast Asia due to its multiple health benefits, different tastes, and special flavor.[3] Pu-erh tea is produced from the sun-dried leaves of *Camellia sinensis* var. assamica in Yunnan province, China. Due to the different processes, pu-erh tea can be categorized into raw pu-erh tea (RAPT, directly compressed and shaped into cake) and ripened pu-erh tea (RIPT, pile-fermented by microorganisms). The participation of the pile-fermentation process is the biggest difference between RIPT and RAPT, and brings great distinctions on infusion colors and tastes,[5] even the chemical constituents and biological activities in our study. Currently, some studies have reported the anti-diabetic effect of pu-erh tea. Wang *et al.* found that flavanols from the water extract of pu-erh tea showed an inhibition effect on α-glucosidase, suggesting potential hypoglycemic effects.[6] In the study of Deng *et al.*, a single administration of polysaccharides from pu-erh tea decreased the postprandial blood sugar in mice, and the mechanism was due to the inhibition of α-glucosidase.[7] Huang *et al.* reported that the 95% ethanol precipitate and ethyl acetate fractions of pu-erh tea showed remarkable inhibition against α-glycosidase *in vitro*.[8] The above studies are only focused on the beneficial effects of RIPT, and the form of a single administration could not simulate the general drinking habit in daily life.

Therefore, a comparative study between RIPT and RAPT was carried out on pharmacological activity and chemical constituent in our research. The anti-diabetic activities of RIPT and RAPT were evaluated in streptozotocin-induced diabetic Wistar rats. Then, the constituents of the RIPT and RAPT were identified. Besides, as the low bioavailability of active constituents from tea[9,10] and the growing evidences on the effect of gut microbiota on diabetes,[11,12] the 16S rRNA analysis was carried out to investigate the effects of RIPT on the gut microbiota.

2 Materials and methods

2.1 Source of pu-erh tea samples

Six batches of samples, including three RIPTs and three RAPTs, were collected from the same production place, Yiwu district,

[a]Beijing Institute of Radiation Medicine, No. 27 Taiping Road, Haidian District, Beijing 100850, China. E-mail: mabaiping@sina.com; Tel: +86-010-66930282

[b]School of Life Science and Biotechnology, Dalian University of Technology, Dalian 116024, Liaoning, China

[c]Beijing University of Chinese Medicine, Beijing 100029, China

[d]Annoroad Gene Technology Co., Ltd, Beijing 100176, China

† Electronic supplementary information (ESI) available. See DOI: 10.1039/c8ra09259a

Open Access Article. Published on 23 January 2019. Downloaded on 1/13/2026 11:41:34 AM. This article is licensed under a Creative Commons Attribution-NonCommercial 3.0 Unported Licence.

Dai Autonomous Prefecture of Xishuangbanna, Yunnan province, China.

2.2 Preparations of extracts from RIPT and RAPT

The tea extract was prepared with process similar to the general drinking habit in China. Each sample (1000 g) was extracted twice with 10 L and 7 L distilled water each for one hour at 100 °C, respectively. After filtration, two solutions were combined and concentrated at 55 °C, and then lyophilized.

2.3 Animals and treatment

Male Wistar rats (180–220 g) were purchased from Beijing Vital River Laboratory Animal Technology Co., Ltd. (Beijing, China). The rats were provided with a standard rodent diet and free access to water, and were maintained at a temperature of 20–22 °C. The animals and protocols for this study were approved by international ethical guidelines and the Institutional Animal Care and Use Committee of Dalian Medical University, with the permission number of SCXK 2013-0003.

The nongenetic diabetic rat model was established following the methods published previously.[13,14] Seventy rats were fed with a high-fat, high-sugar diet (HFHSD) (D12451, 45% calories from fat) instead of standard chow, and had free access to water. On Day 14, the rats were injected intraperitoneally with 40 mg kg^{-1} streptozocin (STZ, Sigma-Aldrich Chemical Co., St. Louis, USA.). On Day 21 and Day 28, oral glucose tolerance tests (OGTTs) were performed. A total of 30 rats met the standard of diabetes, with 2h-PBG levels ranging from 16.7 mmol mL^{-1} to 24.0 mmol mL^{-1} in both OGTTs, and were selected as diabetic rats. Another 5 rats were fed a normal diet as the negative control.

In this set of experiments, normoglycemic rats were fed a standard chow diet and were given vehicle alone (0.5% CMC-Na) daily by oral gavage (NM). The diabetic rats fed with a HFHSD were divided into six groups ($n = 5$ for each group) and were treated with either vehicle (DM), 500 mg kg^{-1} of metformin in vehicle (Met), 600 mg kg^{-1} of extract from RIPT (IH), 120 mg kg^{-1} of extract from RIPT (IL), 800 mg kg^{-1} of extract from RAPT (AH), and 160 mg kg^{-1} of extract from RAPT (AL) in vehicle for 6 weeks.

2.4 OGTT assay

After 14 hour fasting, the rats were orally administered with 2 g kg^{-1} glucose. Blood samples were collected from the tail vein and the levels of FBG and 2h-PBG were measured using the Roche glucometer at week 6.

2.5 Biochemical analyses

The OGTT was performed every week. At the end of the study, the rats were sacrificed after 16 h of fasting. The blood samples were collected and centrifuged at 4000 g for 5 min at 4 °C to obtain the plasma. Fasting plasma insulin (FINS) levels were determined using ELISA kits (Abcam, USA). The values of hemoglobin A1c (HbA1c), total cholesterol (TC), and triglyceride (TG) in plasma were measured according to commercially available kits purchased from Jiancheng Institute of Biotechnology, Nanjing, China.

2.6 Analysis of chemical constituents

In this study, 10 mg of powders were accurately weighed and suspended in 1 mL water, respectively. The samples were then vortexed 1 min, followed by centrifugation for 10 min at 15 000 rpm at 4 °C. 2 μL of the ultra-performance liquid chromatography coupled with a hybrid quadrupole time-of-flight mass spectrometry (UHPLC-Q-TOF/MS) analysis.

An Acquity UPLC system (Waters Corp., Milford, MA, USA) coupled with a Synapt MS system (Waters Corp., Milford, MA, USA) was used. The samples were separated on a Waters Acquity UPLC HSS T3 column (100 × 2.1 mm, 1.8 μm). The mobile phase consisted with (A) 0.1% formic acid solution (v/v) and (B) acetonitrile, while the gradient program was as follows: 98% (A) in 0–1 min; 98–96% (A) in 1–2 min; 96–95% (A) in 2–4 min; 95–93% (A) in 4–6 min; 93–92% (A) in 6–9 min; 92–90% (A) in 9–11 min; 90–86% (A) in 11–15 min; 86% (A) in 15–16 min; 86–83% (A) in 16–19 min; 83–76% (A) in 19–22 min; 76–60% (A) in 22–25 min; 60–43% (A) in 25–26 min; 43–42% (A) in 26–27 min; 42–5% (A) in 27–28 min; 5% (A) in 28–28.5 min. The mobile phase flow rate was 0.6 mL min^{-1} with the column temperature at 45 °C. The wavelength of PDA detector was set from 190 to 400 nm, and 280 nm was set at the monitoring wavelength.

The data acquisition mode was MS^E. Each extract was directed to a trap mass spectrometer with an electrospray interface (ESI) operating in full scan MS mode from m/z 50 to 1500 Da. Mass spectra were acquired in both negative and positive modes with the source temperature was 100 °C, the desolvation temperature was 450 °C, and desolvation gas flow of 850 L h^{-1}. The capillary voltage was 3 kV. At low CE scan, the cone voltage was 30 V, and the collision energy was 6 eV (trap) and 4 eV (transfer). At high CE scan, the cone voltage was 30 V, and the collision energy was 50–65 eV (trap) and 15 eV (transfer). Leucine-enkephalin was used as lock mass.

Standards, including gallic acid (>98%), catechin (>98%), catechingallate (>98%), epicatechin (>98%), epicatechingallate (>98%), epigallocatechin (>98%), epigallocatechin gallate (>98%), gallocatechingallate (>98%), (+)-gallocatechin (>98%), theophylline (>98%), procyanidin B1 (>97%), were purchased from Chengdu Biopurify Phytochemicals Ltd. Caffeine (>98%) was isolated previously. Its structure and purity were confirmed by NMR spectra and high-performance liquid chromatography coupled with evaporative light scattering detection (HPLC-ELSD).

Acetonitrile (HPLC grade) was purchased from Fisher Scientific Co. (Loughborough, UK). Distilled water was purchased from Watsons. Formic acid (HPLC grade) was purchased from Acros Co. Ltd. (St. Louis, MO, USA). Other reagents were obtained commercially in analytical purity (Beijing, China).

2.7 Feces collection, bacterial DNA extraction, PCR amplification and sequencing

At the end of the experiment, feces of rats from NM, DM, Met and IH were collected into sterilized plastic tubes and stored at −80 °C until tested.

 This journal is © The Royal Society of Chemistry 2019

Open Access Article. Published on 23 January 2019. Downloaded on 1/13/2026 11:41:34 AM.
This article is licensed under a Creative Commons Attribution-NonCommercial 3.0 Unported Licence.

Bacterial DNA was extracted from the fecal contents of the rat. The purity and concentration of extracted bacterial DNA were tested by NanoPhotometer spectrophotometer and Qubit 2.0 Flurometer, respectively.

The V3–V4 hypervariable regions of the bacteria 16S rRNA gene were amplified with primers 341F (5′-CCTACGGGNGGCWGCAG-3′) and 805R (5′-GACTACHVGGGTATCTAATCC-3′) by thermocycler PCR system (GeneAmp 9700, ABI, USA). All PCR reactions were carried out in 30 μL reactions with 15 μL of Phusion High-Fidelity PCR Master Mix (New England Biolabs); 0.2 μmol mL^{-1} of forward and reverse primers, and about 10 ng template DNA. Thermal cycling consisted of initial denaturation at 95 °C for 3 min, followed by 25 cycles of denaturation at 95 °C for 30 s, annealing at 55 °C for 30 s, and elongation at 72 °C for 30 s. Then final extension at 72 °C for 10 min. Mix same volume of 1× loading buffer (contained SYB green) with PCR products and operate electrophoresis on 2% agarose gel for detection. Samples with bright main strip around 460 bp (V3 + V4) were chosen for further experiments. PCR products were mixed in equidensity ratios. Then, mixture PCR products were purified with GeneJET Gel Extraction Kit (Thermo Scientific). Sequencing libraries were generated using NEB Next Ultra DNA Library Prep Kit for Illumina (NEB, USA) following manufacturer's recommendations and index codes were added. The library quality was assessed on the Qubit@ 2.0 Fluorometer (Life Technologies, CA, USA) and Agilent Bioanalyzer 2100 system. At last, the library was sequenced on an Illumina MiSeq platform and 250 bp paired-end reads were generated.

2.8 Bioinformatics analysis

Raw reads were filtered to remove the adapter-polluted reads, low quality reads (average quality lower than 19 with PHRED algorithm) and the reads with N bases exceeding 5%. Then, the clean paired reads were spliced with the PEAR software[15] into merged sequences based on sequence overlap. After merging, the sequence Chimeras were removed, and the sequences were clustered into operational taxonomic units (OTUs) by UCLUST[16] with a threshold of 97% pairwise identity. Then, the Silva database (release 128, http://www.arb-silva.de) was used to annotate the taxonomic information. After OTUs annotation, the abundance information was normalized with a standard sequence number according to the sample which had the least sequences. Then, the normalized output data were applied to the subsequent analyses, such as alpha and beta diversity. The community richness and diversity estimations, such as Chao1, ACE and the Shannon index, were calculated by QIIME version 1.8.0 (ref. 17) and displayed utilizing R software. In the beta diversity analysis, the cluster analysis was utilized with principal coordinate analysis (PCoA) based on matrix of Taxonomic OTU, by using R software with ggplot2 and ade4 package. In the PCoA analysis, the distance matrices of weighted or unweighted UniFrac[18] among samples were also needed.

3 Statistical analysis

The data in the negative mode of principal component analysis (PCA) and orthogonal partial least squares discriminant analysis (OPLS-DA) were processed by the MarkerLynx V4.1 software (Waters Co., Milford, USA). The method parameters were set as follows: mass range 100–1500 Da, retention time range 0.2–25.0 min, mass tolerance 5.0 ppm, peak width at 5% height was 1.00 s, peak-to-peak baseline noise 0.00, noise elimination level was set at 6.00 and retention time tolerance was set at 0.01 min. The results were visualized in a score plot to show group clusters, and a variable importance in projection (VIP)-plot to show variables contributing to the classification.

The statistical analysis was performed using SPSS 17.0. Comparisons between groups were analyzed using one-way ANOVA followed by Fisher LSD multiple comparison. $p < 0.05$ was considered statistically significant.

4 Results

4.1 Effects of RAPT and RIPT extracts on the diabetes indices and lipid profiles

After a single injection of STZ and HFHSD induction, the levels of 2h-PBG and FBG were significantly higher in the DM group, compared with those of the NM group (Fig. 1A and B). Metformin, a positive control, significantly lowered the levels of 2h-PBG in diabetic rats. The 2h-PBG lowering effects in the Met, IH and IL groups were significantly observed compared with the DM group, while no significant 2h-PBG-lowering effect was observed in the AH and AL group. Compared with the DM group, the FBG level of the Met group was decreased but not significant. The RIPT administration significantly decreased the FBG level with a dose-dependent pattern in diabetic rat. Meanwhile no significantly differences were observed on the FBG levels of the AH and AL groups compared with the DM group.

The level of FINS was significantly increased in the IL group compared with that of the DM group, but showed no significance when compared with that of the NM group (Fig. 1C). Moreover, the high level of HbA1c in diabetic rats was improved by RIPT administration which had similar effect to metformin (Fig. 1D).

The levels of plasma TC (Fig. 1E) and TG (Fig. 1F) were significantly higher in the DM group, compared to those of the NM group. After 6 week treatment, the metformin, RIPT and RAPT significantly decreased the plasma TC and TG in diabetic rats, respectively. The effect on plasma TG showed a dose-dependent pattern.

4.2 Chemical profiles and different markers of the extracts from RAPT and RIPT

The extract of RAPT and RIPT were analyzed in both negative and positive ion modes with the same LC conditions. Based on exact mass, fragment ions, retention times, published literatures, and comparison with the standard references, 66 major peaks in both negative and positive ion modes of the pu-erh tea were identified, as summarized in Table 1, including 45 components in the RIPT, and 49 chemical components in the RAPT. As shown in Table 1, 17 peaks were detected in RIPT only, including a series of puerins, such as peak 13, 29, 33, 34, 43, 46,

Open Access Article. Published on 23 January 2019. Downloaded on 1/13/2026 11:41:34 AM.
This article is licensed under a Creative Commons Attribution-NonCommercial 3.0 Unported Licence.

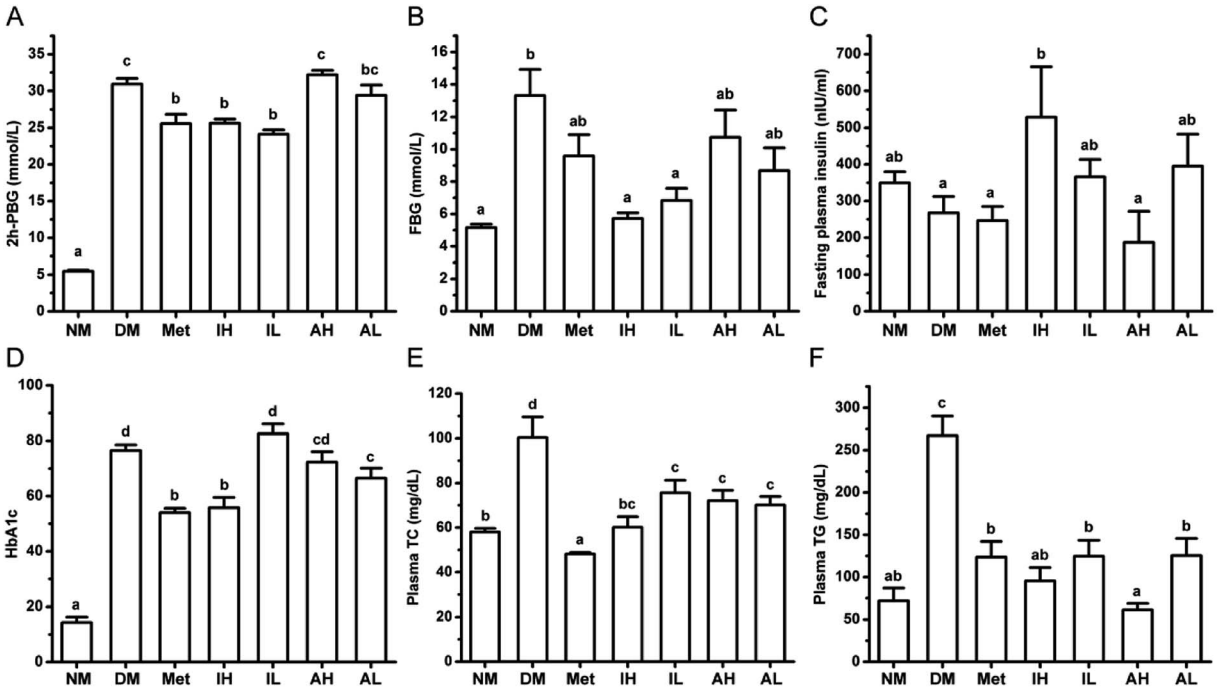

Fig. 1 The effects of RIPT and RAPT on diabetic indexes in diabetic rats. The 2h-PBG (A), FBG (B), FINS (C), HbA1c (D), plasma TC (E), and plasma TG (F) of the rats after 6 week administration. All of the results were expressed as the mean ± SEM ($n = 5$). Values sharing a common letter (a, b, c, and d) in each comparison did not show any statistically significant differences accessed by one-way ANOVA ($p < 0.05$).

47, and 50. Meanwhile, 21 peaks were detected in RAPT only. The rest of 28 peaks were detected in both RIPT and RAPT, the base peak ion (BPI) chromatograms of the RAPT and RIPT by UHPLC-Q-TOF/MS are shown in Fig. 2.

As the great difference between the chromatograms of the RAPT and RIPT, the multivariate statistical methods, including PCA and OPLS-DA, were carried out to find the different components during the pile-fermentation process, additionally. As shown in Fig. 3A, samples were segregated into two groups from the score plot. And the components with the VIP value greater than 2.5 were considered as potential different markers (Fig. 3B), as a result, 26 major different components were identified during the pile-fermentation process (Table 1), including some puerins, such as puerin II (peak 47), III (peak 50), and IV (peak 55).

UHPLC-PDA was used to explain the changes of relative contents caused by pile-fermentation process. A database based on identified components and PDA chemometric data were built. Although quercetin and kaempferol were also mutual components in two kinds of pu-erh tea, the relative content of these two components was not compared as their low content in pu-erh tea and the low response value at 280 nm. Therefore, this database consisted of 26 identified components, and the result was shown in Table 2. As the result, the contents of shared peaks, such as epigallocatechin, catechin, epicatechin and epigallocatechin gallate, were decreased after fermentation except for quinic acid, gallic acid, theophylline or its isomers, caffeine, apigenin-6-C-α-L-arabinopyranosyl-8-C-β-D-glucopyranoside, and ellagic acid. At the same time, puerin I-VIII, a kind of characteristic components, were produced during the fermentation. The corresponding reactions were complex.

4.3 The overall structural changes of the gut microbiota regulated by RIPT intervention

After 6 week administration, as the outstanding pharmaceutical effect of IH, feces of rats in the IH group togethering with those from the NM, DM and Met groups were collected for the gut microbiota analysis. A total of 957 056 high-quality sequences from V3–V4 hypervariable region of the bacterial 16S rRNA gene were collected from 20 samples. The number of average sequence was 47 852, while the maximum number and minimum number were 53 882 and 39 395, respectively. For the length, the average number was 450 bp. With a threshold of 97% pairwise identity, all the sequences were clustered into 667 OTUs. Then, 144 genera or the next higher taxonomic ranks were identified from Silva Database.

To identify the similarities of gut microbiota between the samples of the NM, DM, Met and IH groups, Bray–Curtis distance was performed based on OTU abundance and presented as a hierarchical clustering tree using the data (Fig. 4A). The result showed that samples from each group could be grouped into three clusters, including the NM, DM and treatment (groups treated by IH or metformin) clusters. Among the clusters, the grouped IH and Met samples indicated that they showed similar bacteria compositions. Meanwhile, weighted and unweighted Unifrac distances both indicated samples were significantly separated into three groups, including the NM, DM and treatment (groups treated by IH or metformin) groups

Open Access Article. Published on 23 January 2019. Downloaded on 1/13/2026 11:41:34 AM.
This article is licensed under a Creative Commons Attribution-NonCommercial 3.0 Unported Licence.

Table 1 Compounds determined by UHPLC-Q-TOF/MS in the pu-erh tea extracts

No.	Rt (min)	Formula	$[M-H]^-$ experimental	$[M-H]^-$ theoretical	Error (mD)	Identification	Source[b]		VIP value
							RAPT	RIPT	
1	0.48	$C_7H_{12}O_6$	191.0576	191.0556	2.0	Quinic acid	+	+	2.52395
2	0.91	$C_{14}H_{16}O_{10}$	343.0668	343.0665	0.3	Theogallin or its isomers	+	+	NA
3	0.95	$C_{13}H_{16}O_{10}$	331.0689	331.0665	2.4	Gallic acid-4-*O*-glucoside or its isomers	+	–	2.703
4	1.21	$C_{13}H_{16}O_{10}$	331.0667	331.0665	0.2	Gallic acid-4-*O*-glucoside or its isomers	+	+	4.92352
5	1.36	$C_7H_6O_5$	169.0154	169.0137	1.7	Gallic acid	+	+	2.69024
6	1.47	$C_{13}H_{16}O_{10}$	331.0637	331.0665	−2.8	Gallic acid-4-*O*-glucoside or its isomers	+	–	NA
7	1.77	$C_{14}H_{16}O_{10}$	343.0679	343.0665	1.4	Theogallin	+	+	4.2577
8	2.33	$C_{14}H_{16}O_{10}$	343.0670	343.0665	0.5	Theogallin or its isomers	+	+	3.26224
9	2.95	$C_{15}H_{14}O_7$	305.0668	305.0661	0.7	Gallocatechin	+	+	3.911
10	3.18	$C_7H_8N_4O_2$	181.0706	181.0726	−2.0	Theophylline or its isomers[a]	+	+	NA
11	4.02	$C_{16}H_{18}O_9$	353.0873	353.0873	0.0	Chlorogenic acid	+	+	2.61641
12	4.28	$C_7H_8N_4O_2$	179.0559	179.0569	−1.0	Theophylline or its isomers	+	+	NA
13	4.54	$C_{22}H_{24}O_7$	399.1442	399.1444	−0.3	Puerin A or its isomers	–	+	NA
14	5.12	$C_{16}H_{14}O_9$	349.0559	349.0560	−0.1	6-Carboxyl-(−)-gallocatechin or its isomers	–	+	NA
15	5.8	$C_{15}H_{14}O_7$	305.0660	305.0661	−0.1	Epigallocatechin	+	+	4.30649
16	6.1	$C_{15}H_{14}O_6$	289.0713	289.0712	0.1	Catechin	+	+	4.13423
17	6.24	$C_{37}H_{30}O_{18}$	761.1342	761.1354	−1.2	Theasinensin B	+	–	NA
18	6.48	$C_{16}H_{18}O_9$	353.0862	353.0873	−1.1	3-*O*-Caffeoylquinic acid or its isomers	+	+	NA
19	6.76	$C_{20}H_{20}O_{14}$	483.0780	483.0775	0.5	1,6-Di-*O*-galloyl-β-D-glucopyranose or its isomers	+	–	NA
20	6.88	$C_8H_{10}N_4O_2$	195.0895	195.0882	1.3	Caffeine[a]	+	+	NA
21	7.01	$C_{20}H_{20}O_{14}$	483.0781	483.0775	0.6	1,6-Di-*O*-galloyl-β-D-glucopyranose or its isomers	+	–	2.84282
22	7.22	$C_{16}H_{18}O_9$	353.0859	353.0873	−1.4	3-*O*-Caffeoylquinic acid or its isomers	+	+	NA
23	7.56	$C_{30}H_{26}O_{12}$	577.1343	577.1346	−0.3	Procyanidin B1	+	–	4.41889
24	8.04	$C_{30}H_{26}O_{12}$	577.1352	577.1346	0.6	The isomer of procyanidin B1	+	–	NA
25	8.21	$C_{37}H_{30}O_{17}$	745.1422	745.1405	1.7	Epicatechin-(4β-8)-epigallocatechin-3-*O*-gallate or its isomers	+	–	NA
26	8.42	$C_{30}H_{26}O_{12}$	577.1387	577.1346	4.1	Procyanidin B2	+	–	NA
27	8.51	$C_{16}H_{14}O_9$	349.0556	349.0560	−0.4	6-Carboxyl-(−)-gallocatechin or its isomers	–	+	NA
28	9.04	$C_{37}H_{30}O_{17}$	745.1418	745.1405	1.3	Epicatechin-(4β-8)-epigallocatechin-3-*O*-gallate or its isomers	+	+	NA
29	9.3	$C_{21}H_{23}NO_8$	416.1342	416.1345	−0.3	Puerin VII	–	+	NA
30	9.3	$C_{16}H_{14}O_8$	333.0603	333.0610	−0.7	8-Carboxyl-(+)-catechin or its isomers	—	+	2.89648
31	9.49	$C_{15}H_{14}O_6$	289.0690	289.0712	−2.2	Epicatechin	+	+	4.72175
32	9.86	$C_{22}H_{18}O_{11}$	457.0789	457.0771	1.8	Epigallocatechin gallate	+	+	3.74396
33	10.76	$C_{21}H_{23}NO_8$	416.1320	416.1345	−2.5	Puerin V	–	+	NA
34	11.62	$C_{21}H_{23}NO_8$	416.1364	416.1345	1.9	Puerin VIII	–	+	NA
35	11.64	$C_{37}H_{30}O_{16}$	729.1465	729.1456	0.9	Epicatechin-(4β-8)-epicatechin 3-gallate	+	–	NA
36	11.71	$C_{22}H_{18}O_{11}$	457.0784	457.0771	1.3	Gallocatechin gallate	+	–	4.03217
37	12.14	$C_{27}H_{24}O_{18}$	635.0878	635.0884	−0.6	1,4,6-Tri-*O*-galloyl-β-D-glucopyranose or its isomers	+	–	NA
38	12.22	$C_{29}H_{48}O$	411.3631	411.3627	0.4	α-Spinasterol or its isomers	–	+	NA
39	12.31	$C_{27}H_{30}O_{15}$	593.1515	593.1506	0.9	Kaempferol-3-*O*-rutinoside or its isomers	–	+	NA
40	12.42	$C_{37}H_{30}O_{16}$	729.1478	729.1456	2.2	Epicatechin-(4α-8)-epicatechin-3′-gallate	+	–	NA
41	12.5	$C_{14}H_{11}NO_6$	288.0509	288.0508	0.1	*N*-(3,4-Dihydroxybenzoyl)-3,4-dyhydrobenzamide	–	+	NA
42	12.76	$C_{16}H_{14}O_8$	333.0601	333.0610	−0.9	8-Carboxyl-(+)-catechin or its isomers	–	+	2.56147
43	12.98	$C_{21}H_{23}NO_8$	416.1363	400.1396	1.8	Puerin VI	–	+	NA
44	13.19	$C_{21}H_{20}O_{13}$	479.0820	479.0826	−0.6	Myricetin-3-*O*-β-D-galactopyranoside	+	–	NA

Open Access Article. Published on 23 January 2019. Downloaded on 1/13/2026 11:41:34 AM.
This article is licensed under a Creative Commons Attribution-NonCommercial 3.0 Unported Licence.

Table 1 (*Contd.*)

No.	Rt (min)	Formula	$[M-H]^-$ experimental	$[M-H]^-$ theoretical	Error (mD)	Identification	Source[b] RAPT	RIPT	VIP value
45	13.49	$C_{27}H_{24}O_{18}$	635.0880	635.0884	−0.4	1,4,6-Tri-*O*-galloyl-β-D-glucopyranose or its isomers	+	—	3.39172
46	13.59	$C_{21}H_{22}NO_7$	400.1398	400.1396	0.2	Puerin I	−	+	NA
47	14.07	$C_{21}H_{22}NO_7$	400.1403	400.1396	0.7	Puerin II	−	+	2.57155
48	14.28	$C_{26}H_{28}O_{14}$	563.1409	563.1401	0.8	Apigenin-6-C-α-L-arabinopyranosyl-8-C-β-D-glucopyranoside	+	+	2.80337
49	14.56	$C_{22}H_{18}O_{10}$	441.0818	441.0822	−0.4	Epicatechin gallate	+	+	4.5466
50	14.84	$C_{21}H_{22}NO_7$	400.1391	400.1396	−0.5	Puerin III	−	+	3.78329
51	15.13	$C_{14}H_6O_8$	300.9951	300.9984	−3.3	Ellagic acid	+	+	4.0874
52	15.36	$C_{27}H_{30}O_{16}$	609.1477	609.1456	2.1	The isomer of rutin	+	+	NA
53	15.47	$C_{22}H_{18}O_{10}$	441.0835	441.0822	1.3	Catechin gallate	+	−	4.36602
54	15.87	$C_{27}H_{30}O_{16}$	609.1472	609.1456	1.6	Rutin	+	−	NA
55	15.92	$C_{21}H_{22}NO_7$	400.1387	400.1396	−0.9	Puerin IV	−	+	4.23005
56	16.04	$C_{21}H_{20}O_{12}$	463.0873	463.0877	−0.4	Quercetin-3-*O*-glucoside	+	+	NA
57	16.5	$C_{33}H_{40}O_{20}$	755.2036	755.2035	0.1	Quercetin-4′-*O*-α-L-rhamnopyranosyl-3-*O*-α-L-rhamnopyranosyl-(1→6)-β-D-glucopyranoside or its isomers	+	−	NA
58	17.05	$C_{27}H_{30}O_{15}$	593.1529	593.1506	2.3	Kaempferol-3-*O*-rutinoside or its isomers	+	+	NA
59	17.42	$C_{33}H_{40}O_{20}$	755.2067	755.2035	3.2	Quercetin-4′-*O*-α-L-rhamnopyranosyl-3-*O*-α-L-rhamnopyranosyl-(1→6)-β-D-glucopyranoside or its isomers	+	−	NA
60	17.44	$C_{21}H_{20}O_{11}$	447.0927	447.0927	0.0	Luteolin-7-*O*-glucoside	+	−	NA
61	17.76	$C_{22}H_{18}O_9$	425.0832	425.0873	−4.1	Epiafzelechin-3-*O*-gallate	+	−	NA
62	18.26	$C_{33}H_{40}O_{19}$	739.2134	739.2086	4.8	Kaempferol-3-*O*-[α-L-rhamnopyranosyl-(1→3)-α-L-rhamnopyranosyl-(1→6)-β-D-glucopyranoside]	−	+	NA
63	18.28	$C_{27}H_{30}O_{15}$	593.1534	593.1506	2.8	Kaempferol-3-*O*-rutinoside or its isomers	+	+	NA
64	18.49	$C_{21}H_{20}O_{11}$	447.0919	447.0927	−0.8	Kaempferol-3-*O*-glucoside	+	+	2.78936
65	22.11	$C_{15}H_{10}O_7$	301.0346	301.0348	−0.2	Quercetin	+	+	NA
66	23.84	$C_{15}H_{10}O_6$	285.0419	285.0399	2.0	Kaempferol	+	+	NA

[a] Detected in the positive mode. [b] "+" means the compound was detected in that source, while "−" means not.

This journal is © The Royal Society of Chemistry 2019

Open Access Article. Published on 23 January 2019. Downloaded on 1/13/2026 11:41:34 AM.
This article is licensed under a Creative Commons Attribution-NonCommercial 3.0 Unported Licence.

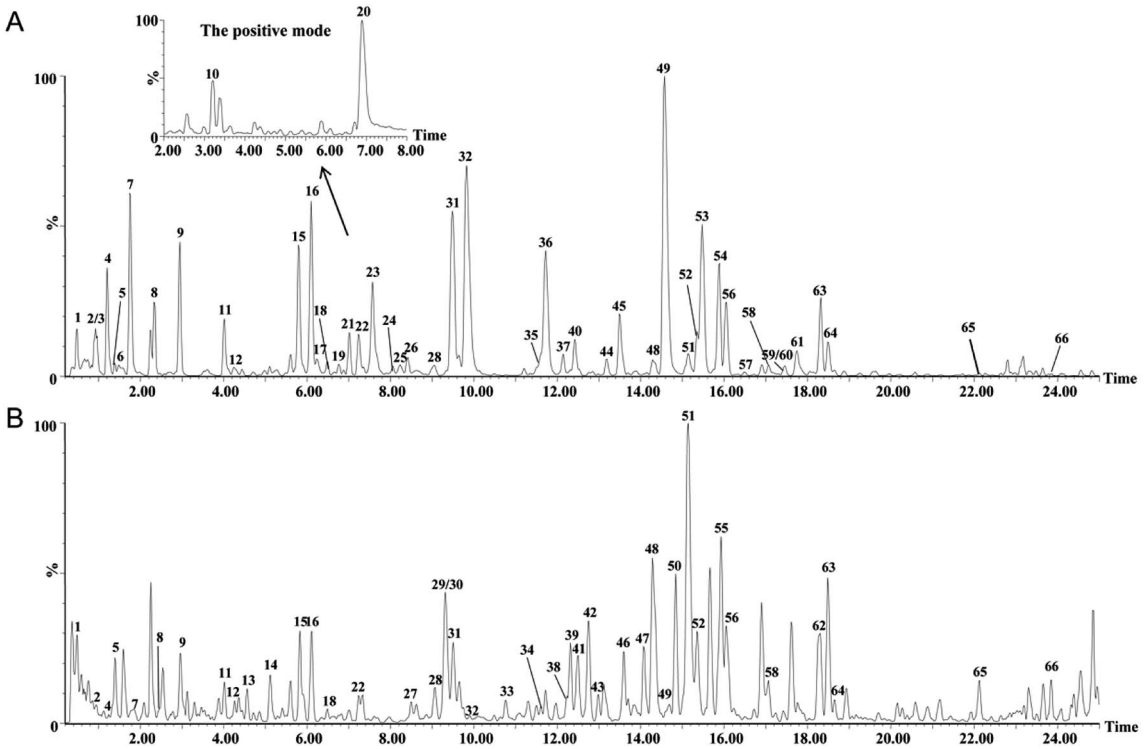

Fig. 2 The BPI chromatograms of the extracts from the negative mode in RAPT (A) and RIPT (B) analyzed by UHPLC-Q-TOF/MS.

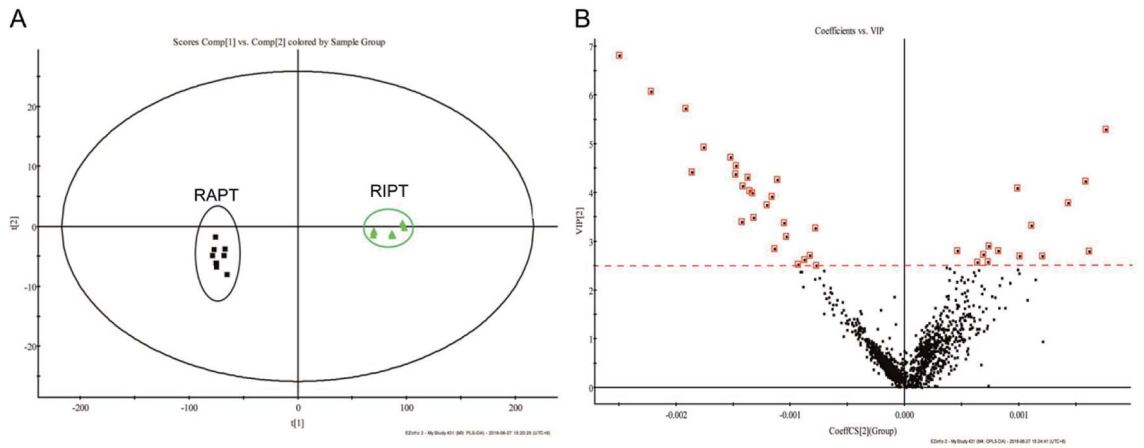

Fig. 3 PCA (A), VIP (B) plot of the extracts from the negative mode in RIPT and RAPT analyzed by UHPLC-Q-TOF/MS.

(Fig. 4B and C). This result was consistent with the results of hierarchical clustering tree. Besides, PC1 values were respectively 40.88% and 84.82% in PCoA plots of weighted and unweighted Unifrac distances, indicating PC1 could reflect the treatment effect on shaping the structure of gut microbiota.

In order to understand the detail microbial changes, the gut microbiota structure was analyzed at different taxonomic levels including phylum and genus level (Fig. 4D). At the phylum level, most of the microbiota was from *Firmicutes* (51.96% in all identified reads) and *Bacteroidetes* (35.30% in all identified reads). After being induced by STZ and HFHSD, the increased relative abundance of *Firmicutes* and the decreased relative abundance of *Bacteroidetes* were observed in diabetic rats. Therefore, the *Bacteroidetes*/*Firmicutes* (B/F) ratio was decreased in the DM group (0.48 ± 0.16) compared to that of the NM group (1.08 ± 0.23), and was slightly reverted in the Met and IH groups (Met, 0.79 ± 0.36; IH, 0.57 ± 0.12). The treatment with metformin or RIPT increased *Bacteroidetes* relative abundance and B/F ratio. Due to the differences between samples, no significant changes were observed. Besides, the *Actinobacteria* relative abundance was significantly increased in the DM group ($4.286\% \pm 3.97\%$) and reverted by metformin or RIPT treatment (Met, $0.08003\% \pm 0.0747\%$; IH, $0.04494\% \pm 0.02207\%$).

Open Access Article. Published on 23 January 2019. Downloaded on 1/13/2026 11:41:34 AM.
This article is licensed under a Creative Commons Attribution-NonCommercial 3.0 Unported Licence.

Table 2 Content comparisons of mutual components between RAPT and RIPT by UHPLC-PDA[a]

Peak no.	Rt (min)	Peak area		Changes in RIPT[b]	p-value
		RIPT	RAPT		
1	0.48	5413.78 ± 644.21	819.11 ± 162.87	↑	5.4×10^{-13}
2	0.91	743.89 ± 402.95	1627.22 ± 680.07	↓	4.0×10^{-3}
4	1.21	540.11 ± 223.95	5509.22 ± 1136.93	↓	7.5×10^{-10}
5	1.36	27 794.89 ± 14 100.32	20 960.56 ± 4531.10	↑	1.9×10^{-1}
7	1.77	1665.11 ± 266.70	31 399.89 ± 1296.43	↓	4.5×10^{-21}
8	2.33	129.56 ± 113.96	3462.00 ± 777.84	↓	8.8×10^{-10}
9	2.95	98.11 ± 8.16	1196.22 ± 127.16	↓	1.8×10^{-14}
10	3.18	10 456.22 ± 248.83	5320.44 ± 1293.96	↑	3.0×10^{-9}
11	4.02	193.78 ± 79.17	2829.00 ± 259.68	↓	2.7×10^{-15}
12	4.28	600.33 ± 155.54	171.89 ± 45.19	↑	6.2×10^{-7}
15	5.8	88.44 ± 2.96	1756.33 ± 492.03	↓	2.2×10^{-8}
16	6.1	299.33 ± 65.45	5488.33 ± 560.78	↓	6.5×10^{-15}
18	6.48	128.67 ± 41.45	1274.00 ± 200.88	↓	1.4×10^{-11}
20	6.88	149 441.78 ± 3758.53	98 945.78 ± 8242.66	↑	1.5×10^{-11}
22	7.22	191.89 ± 18.11	2735.89 ± 203.26	↓	5.3×10^{-17}
28	9.04	486.44 ± 103.20	1557.89 ± 96.01	↓	1.3×10^{-13}
31	9.49	214.78 ± 111.37	9497.00 ± 1907.87	↓	1.2×10^{-10}
32	9.86	68.11 ± 50.40	39 900.56 ± 9011.16	↓	4.8×10^{-10}
48	14.28	277.67 ± 42.04	186.44 ± 53.65	↑	1.0×10^{-3}
49	14.56	188.89 ± 100.50	49 858.67 ± 7605.17	↓	1.3×10^{-12}
51	15.13	3704.67 ± 817.51	2069.56 ± 156.84	↑	2.3×10^{-5}
52	15.36	281.78 ± 56.62	351.33 ± 58.48	↓	2.1×10^{-2}
56	16.04	387.00 ± 175.11	1230.89 ± 127.26	↓	3.0×10^{-9}
58	17.05	173.78 ± 77.95	248.78 ± 58.63	↓	3.5×10^{-2}
63	18.28	395.44 ± 217.17	1378.11 ± 704.96	↓	1.0×10^{-3}
64	18.49	375.56 ± 171.71	761.44 ± 353.08	↓	9.4×10^{-3}

[a] All of the results were expressed as the mean ± SD ($n = 3$). p value was calculated by two-tailed t test. [b] Five key increased components were emphasized with bold arrows.

When compared to the relative abundances of the NM group at the genus level, 26 genera in the DM group were significantly increased, and 29 genera in the DM group were significantly decreased (Table S1†). Among 26 increased genera, 11 genera were significantly decreased by RIPT, and 7 genera were significantly decreased by metformin. Among 29 decreased genera, 4 genera were significant increased by RIPT, and the same 4 genera were also significantly increased by metformin. Some known beneficial genera, such as *lactobacillus*, *Prevotellaceae NK3B31 group*, *Alloprevotella* and *Prevotella_1*, were enriched by RIPT (Table 3).

5 Discussions

In recent years, the anti-diabetic effect of pu-erh tea were widely reported and recognized. Du *et al.* reported that the pu-erh tea extract had beneficial effects on glucose homeostasis and insulin resistance improvement.[4] In this study, the extract of RIPT and RAPT showed alleviation effect of hyperglycemia and hyperlipidemia with more potent activity in RIPT extract. Therefore, the differences on components of two pu-erh teas and modulation effect of RIPT on gut microbiota, which might cause the more effective hypoglycemic result after RIPT treatment, were further investigated.

Compared RIPT with RAPT, the key difference is the manufacture process, specially the microbial pile-fermentation. Many microbes, including *Aspergillus* spp., *Penicllium*, *Rhizopus*, *Saccharomyces*, and *Bacterium*, play a key role in the post-fermentation process of RIPT manufacture, while RAPT is processed with natural aging only. As various effects of different microbes, some components could be dramatically changed during the fermentation process. In RAPT, the main components are catechins, tea polyphenols, soluble sugar.[5] On the contrary, the contents of caffeine, gallic acid was increased after fermentation.[19] Researches have shown that the gallated catechins would have a gradually decomposing process to produce catechins and gallic acid during pile-fermentation, therefore, the content of gallic acid was increased. However, catechins would further reacted during fermentation.[20] In our study, these changes are consistent with published researches. 19 Components were detected in RIPT only, including puerin I-VIII, 8-carboxyl-(+)-catechin or its isomers, *etc.* in this work. As reported by Wang *et al.*, puerin I-VIII came from catechins and theanine through fungal fermentation, and could be quality control markers and authentication for RIPT.[21] The puerin II, III, and IV

Open Access Article. Published on 23 January 2019. Downloaded on 1/13/2026 11:41:34 AM.
This article is licensed under a Creative Commons Attribution-NonCommercial 3.0 Unported Licence.

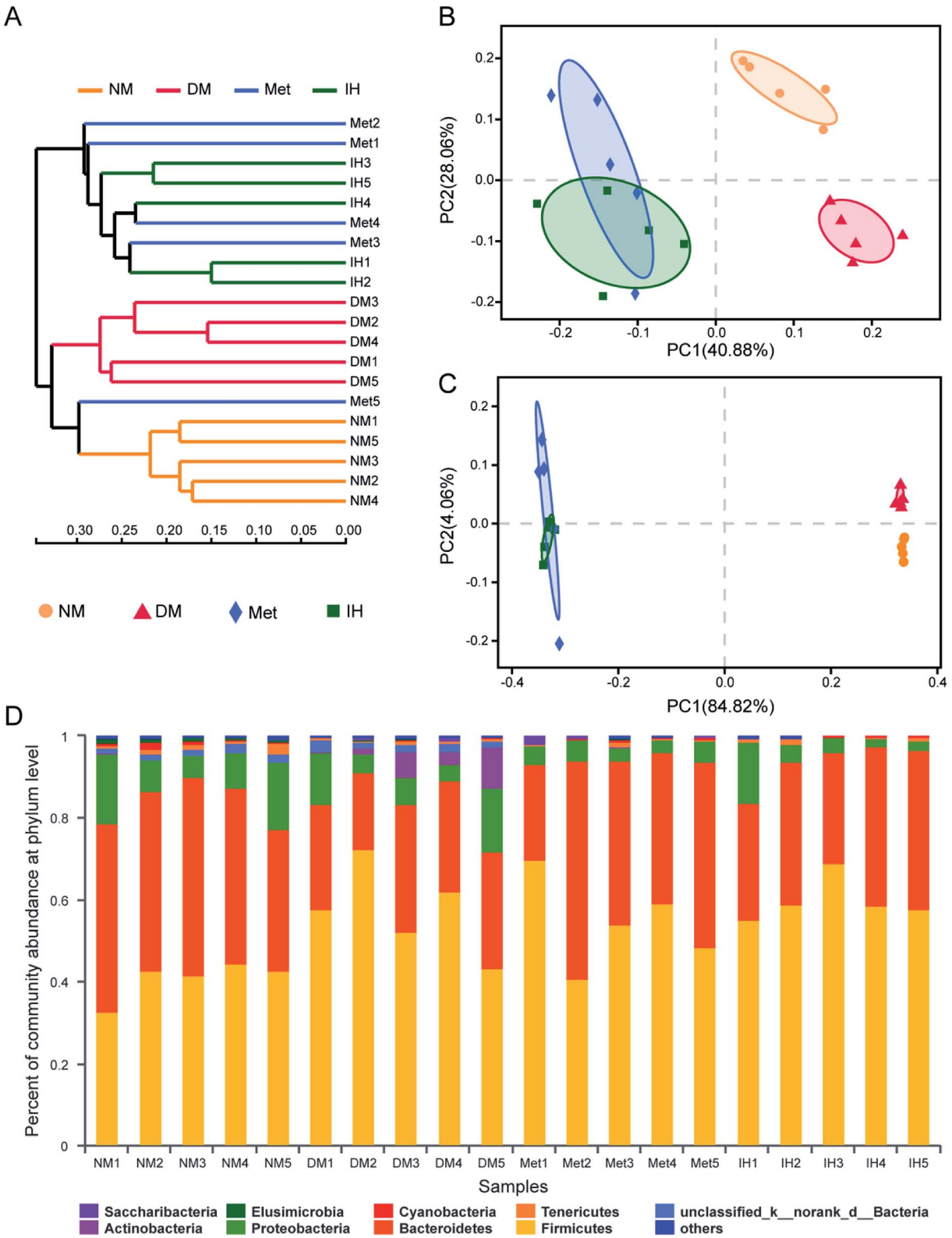

Fig. 4 Overall structural changes of the gut microbiota in response to 6 week administration with RIPT. (A) The cluster for every sample with Bray–Curtis distance. (B) Weighted version of UniFrac-based PCoA plot with PC1 and PC2 at the OTU level. (C) Unweighted version of UniFrac-based PCoA plot with PC1 and PC1 at the OTU level. (D) The relative abundance of phylotypes at the phylum level in different samples.

Open Access Article. Published on 23 January 2019. Downloaded on 1/13/2026 11:41:34 AM.
This article is licensed under a Creative Commons Attribution-NonCommercial 3.0 Unported Licence.

Table 3 Relative abundance of beneficial genera in NM, DM, Met and IH groups after the 6 week administration[a]

	Relative abundance			
Genus	NM	DM	Met	IH
Lactobacillus	0.23 ± 0.14^{a}	0.75 ± 0.26^{a}	5.00 ± 4.37^{a}	19.22 ± 13.17^{b}
Prevotellaceae_NK3B31_group	1.78 ± 0.49^{ab}	0.70 ± 0.48^{a}	5.10 ± 2.51^{b}	4.96 ± 3.90^{b}
Alloprevotella	5.21 ± 3.31^{a}	0.56 ± 0.53^{a}	3.36 ± 5.38^{a}	2.03 ± 1.97^{a}
Prevotella_1	0.85 ± 0.66^{a}	0.58 ± 0.83^{a}	4.36 ± 6.14^{a}	4.51 ± 3.05^{a}

[a] All of the results were expressed as the mean ± SD ($n = 5$). Values sharing a common letter (a and b) in each comparison did not show any statistically significant differences accessed by one-way ANOVA followed by Tukey's *post hoc* test ($p < 0.05$).

were also recognized as markers with VIP value greater than 2.5 for pile-fermentation process in this study. In addition, puerin I was reported to exhibit hypoglycemic and hypolipidemic effect through inhibiting α-glycosidase and activating low-density lipoprotein receptor.[22] Therefore, puerins, especially the puerin I, might contribute to the more potent anti-diabetic effect in RIPT. When compared HPLC-PDA result of mutual components detected in RIPT and RAPT, 6 components, including quinic acid, gallic acid, theophylline or its isomers, caffeine, apigenin-6-C-α-L-arabinopyranosyl-8-C-β-D-glucopyranoside, and ellagic acid, were increased after pile-fermentation. As published research, caffeine could promote the expression of glucose transporter 4 to dispose glucose and result in alleviating diabetes.[23] In our study, caffeine was significantly increased after pile-fermentation, which would be related to the better hypoglycemic effect of RIPT. Arya *et al.* reported that quinic acid down-regulated hyperglycemia, hyperlipidemia, and insulin resistance on diabetic rats induced by STZ.[24] Meanwhile, gallic acid was also report to attenuate insulin resistance and enhances glucose uptake through activating peroxisome proliferator-activated receptor γ and glucose transporter 4, respectively. The increase of gallic acid content in the RIPT in our study would also be relevant to the better hypoglycemic effect. Therefore, these components increased after fermentation might also contribute to the enhanced activities of RIPT. Besides, the increase of insoluble polyphenols and polysaccharides in RIPT was also reported in previous study.[5] They might affect the gut microbiota, and then alleviate diabetes.

To date, the increasing evidences showed that polyphenols and polysaccharides played a probiotic role to modulate gut microbiota, and then ameliorate metabolic syndrome.[25,26] The relationships among tea components, diabetes and gut microbiota attracted our attention. Because of the best hypoglycemic activity of RIPT, the feces of rats from the IH group were collected together with those from the NM, DM, and Met groups, and their modulating effects on gut microbiota were investigated. According to the Bray–Curtis distance and PCoA plots, the overall structure of gut microbiota from the IH group was much more similar to that from the Met group, indicating that the gut microbiota in these two groups might have the similar contribution to anti-diabetic effect. As Wu *et al.* reported, the metformin-altered gut microbiota had benefits to the anti-diabetic effect.[27] When looking into the changes at the phylum level, the increased B/F ratio, which was observed in our study, was reported to exhibit positive effects on attenuating insulin-resistance, diabetes, and obesity.[28,29] Besides, the phylum *Actinobacteria*, which was enriched in the DM group and reversed in the IH group in our study, was reported as a pathogen bacteria which had a higher abundance in the women with gestational diabetes mellitus.[30] When investigating the changes at the genus level, the probiotic role of RIPT to some health-promoting genera, including *lactobacillus*, *Prevotellaceae NK3B31 group*, *Alloprevotella* and *Prevotella_1*, were observed in our study. These increased genera were also reported as probiotics which could ameliorate diabetes through increasing insulin release in glucose tolerant individuals,[31] producing beneficial short chain fatty acids[32] or promoting glucose metabolism.[33] These beneficial effects from gut microbiota potentially related to the increased probiotic components from RIPT, and then enhenced the anti-diabetic effect compared with that of RAPT.

6 Conclusion

This comparative study between RIPT and RAPT exhibited that RIPT extract had more potent anti-diabetic effect than RAPT extract. The differences in chemical profiles were also found by UHPLC-Q-TOF/MS analysis, and might contribute to the activity difference. Among them, 17 newly formed components and the increased components after fermentation, such as quinic acid, gallic acid, caffeine, puerin I and so on, might be the main contributors to the enhanced activities. In addition, the gut microbiota potentially contributed to the enhancement of hypoglycemic activity in RIPT through its probiotic role to some health-promoting genera, including *Lactobacillus*, *Prevotellaceae NK3B31 group*, *Alloprevotella*, *etc.* These results indicated that RIPT could be a functional beverage for alleviating diabetes. The mechanisms involved key components and gut microbiota modulation are needed to be further studied.

Conflicts of interest

The authors have declared no conflicts of interest.

Abbreviations

BPI	Base peak ion
FBG	Fasting blood glucose
FINS	Fasting plasma insulin
GC-MS	Gas chromatography-mass spectrometer
HFHSD	High-fat, high-sugar diet

Open Access Article. Published on 23 January 2019. Downloaded on 1/13/2026 11:41:34 AM.
This article is licensed under a Creative Commons Attribution-NonCommercial 3.0 Unported Licence.

HPLC-ELSD	High-performance liquid chromatography coupled with evaporative light scattering detection
OGTT	Oral glucose tolerance test
OPLS-DA	Orthogonal partial least squares discriminant analysis
OTUs	Operational taxonomic units
PCA	Principal component analysis
PCoA	Principal coordinate analysis
PDA	Photo-diode array
SCFA	Short chain fatty acid
STZ	Streptozocin
TC	Total cholesterol
TG	Triglyceride
UHPLC-Q-TOF/MS	Ultra-performance liquid chromatography coupled with a hybrid quadrupole time-of-flight mass spectrometry
VIP	Variable importance in projection
2h-PBG	Two-hour postprandial blood glucose

Acknowledgements

The authors thank Annoroad Gene Tech. (Beijing) Co., Ltd for their excellent technical assistance. This study was supported by the National Natural Science Foundation of China (No. 81773867).

References

1 W. H. Organization, *Global report on diabetes*, World Health Organization, 2016.
2 N. H. Cho, J. E. Shaw, S. Karuranga, Y. Huang, J. D. da Rocha Fernandes, A. W. Ohlrogge and B. Malanda, *Diabetes Res. Clin. Pract.*, 2018, **138**, 271–281.
3 L. K. Lee and K. Y. Foo, *Food Res. Int.*, 2013, **53**, 619–628.
4 W. H. Du, S. M. Peng, Z. H. Liu, L. Shi, L. F. Tan and X. Q. Zou, *J. Agric. Food Chem.*, 2012, **60**, 10126–10132.
5 H. P. Lv, Y. J. Zhang, Z. Lin and Y. R. Liang, *Food Res. Int.*, 2013, **53**, 608–618.
6 X. Wang, Q. Liu, H. Zhu, H. Wang, J. Kang, Z. Shen and R. Chen, *Acta Pharm. Sin. B*, 2017, **7**, 342–346.
7 Y. T. Deng, S. Y. Linshiau, L. F. Shyur and J. K. Lin, *Food Funct.*, 2015, **6**, 1539–1546.
8 Q. Huang, S. Chen, H. Chen, Y. Wang, Y. Wang, D. Hochstetter and P. Xu, *Food Chem. Toxicol.*, 2013, **53**, 75–83.
9 P. C. H. Hollman, *J. Sci. Food Agric.*, 2000, **80**, 1081–1093.
10 S. Sang, J. D. Lambert and C. S. Yang, *J. Sci. Food Agric.*, 2010, **86**, 2256–2265.
11 G. Blandino, R. Inturri, F. Lazzara, R. M. Di and L. Malaguarnera, *Diabetes Metab.*, 2016, **42**, 303–315.
12 L. Zhao, *Nat. Rev. Microbiol.*, 2013, **11**, 639.
13 R. S. Danda, N. M. Habiba, H. Rincon-Choles, B. K. Bhandari, J. L. Barnes, H. E. Abboud and P. E. Pergola, *Kidney Int.*, 2005, **68**, 2562–2571.
14 B. Zhang, W. Sun, N. Yu, J. Sun, X. Yu, X. Li, Y. Xing, D. Yan, Q. Ding, Z. Xiu, B. Ma, L. Yu and Y. Dong, *J. Funct. Foods*, 2018, **46**, 256–267.
15 J. Zhang, K. Kobert, T. Flouri and A. Stamatakis, *Bioinformatics*, 2014, **30**, 614–620.
16 R. C. Edgar, *Bioinformatics*, 2010, **26**, 2460–2461.
17 J. G. Caporaso, J. Kuczynski, J. Stombaugh, K. Bittinger, F. D. Bushman, E. K. Costello, N. Fierer, A. G. Pena, J. K. Goodrich, J. I. Gordon, G. A. Huttley, S. T. Kelley, D. Knights, J. E. Koenig, R. E. Ley, C. A. Lozupone, D. McDonald, B. D. Muegge, M. Pirrung, J. Reeder, J. R. Sevinsky, P. J. Turnbaugh, W. A. Walters, J. Widmann, T. Yatsunenko, J. Zaneveld and R. Knight, *Nat. Methods*, 2010, **7**, 335–336.
18 C. Lozupone and R. Knight, *Appl. Environ. Microbiol.*, 2005, **71**, 8228–8235.
19 L. Zhang, N. Li, Z. Z. Ma and P. F. Tu, *J. Agric. Food Chem.*, 2011, **59**, 8754–8760.
20 Y. F. Zhu, J. J. Chen, X. M. Ji, X. Hu, T. J. Ling, Z. Z. Zhang, G. H. Bao and X. C. Wan, *Food Chem.*, 2015, **170**, 110–117.
21 W. Wang, L. Zhang, S. Wang, S. Shi, Y. Jiang, N. Li and P. Tu, *Food Chem.*, 2014, **152**, 539–545.
22 X. P. Gu, Z. Wu, F. Y. Jin, B. Pan, Y. F. Zhao, J. Li, J. Zheng and P. F. Tu, *China J. Chin. Mater. Med.*, 2018, **43**, 2339–2344.
23 E. Mukwevho, T. A. Kohn, D. Lang, E. Nyatia, J. Smith and E. O. Ojuka, *Am. J. Physiol.: Endocrinol. Metab.*, 2008, **294**, E582–E588.
24 A. Arya, M. M. Al-Obaidi, N. Shahid, M. I. Bin Noordin, C. Y. Looi, W. F. Wong, S. L. Khaing and M. R. Mustafa, *Food Chem. Toxicol.*, 2014, **71**, 183–196.
25 S. M. Henning, J. Yang, M. Hsu, R. P. Lee, E. M. Grojean, A. Ly, C. H. Tseng, D. Heber and Z. Li, *Eur. J. Nutr.*, 2018, **57**, 2759–2769.
26 Q. Nie, J. Hu, H. Gao, L. Fan, H. Chen and S. Nie, *Food Hydrocolloids*, 2019, **86**, 34–42.
27 H. Wu, E. Esteve, V. Tremaroli, M. T. Khan, R. Caesar, L. Manneras-Holm, M. Stahlman, L. M. Olsson, M. Serino, M. Planas-Felix, G. Xifra, J. M. Mercader, D. Torrents, R. Burcelin, W. Ricart, R. Perkins, J. M. Fernandez-Real and F. Backhed, *Nat. Med.*, 2017, **23**, 850–858.
28 D. E. Roopchand, R. N. Carmody, P. Kuhn, K. Moskal, P. Rojas-Silva, P. J. Turnbaugh and I. Raskin, *Diabetes*, 2015, **64**, 2847–2858.
29 P. J. Turnbaugh, R. E. Ley, M. A. Mahowald, V. Magrini, E. R. Mardis and J. I. Gordon, *Nature*, 2006, **444**, 1027–1031.
30 M. K. W. Crusell, T. H. Hansen, T. Nielsen, K. H. Allin, M. C. Ruhlemann, P. Damm, H. Vestergaard, C. Rorbye, N. R. Jorgensen, O. B. Christiansen, F. A. Heinsen, A. Franke, T. Hansen, J. Lauenborg and O. Pedersen, *Microbiome*, 2018, **6**, 89.
31 M. C. Simon, K. Strassburger, B. Nowotny, H. Kolb, P. Nowotny, V. Burkart, F. Zivehe, J. H. Hwang, P. Stehle and G. Pacini, *Diabetes Care*, 2015, **38**, 1827–1834.
32 X. Wei, J. Tao, S. Xiao, S. Jiang, E. Shang, Z. Zhu, D. Qian and J. Duan, *Sci. Rep.*, 2018, **8**, 3685.
33 P. Kovatcheva-Datchary, A. Nilsson, R. Akrami, Y. S. Lee, F. De Vadder, T. Arora, A. Hallen, E. Martens, I. Bjorck and F. Backhed, *Cell Metab.*, 2015, **22**, 971–982.